

Axisymmetric modes in vertically stratified self-gravitating discs

G. R. Mamatsashvili^{1,2*} and W. K. M. Rice¹

¹ *SUPA, Institute for Astronomy, University of Edinburgh, Blackford Hill, Edinburgh EH9 3HJ, Scotland*

² *Georgian National Astrophysical Observatory, Ilia State University, 2a Kazbegi Ave., Tbilisi 0160, Georgia*

Accepted 2010 April 09. Received 2010 April 08; in original form 2010 February 09

ABSTRACT

We carry out a linear analysis of the vertical normal modes of axisymmetric perturbations in stratified, compressible, self-gravitating gaseous discs in the shearing box approximation. An unperturbed disc has a polytropic vertical structure that allows us to study specific dynamics for subadiabatic, adiabatic and superadiabatic vertical stratifications, by simply varying the polytropic index. In the absence of self-gravity, four well-known principal modes can be identified in a stratified disc: acoustic p-modes, surface gravity f-modes, buoyancy g-modes and inertial r-modes. After classifying and characterizing modes in the non-self-gravitating case, we include self-gravity in the perturbation equations and in the equilibrium and investigate how it modifies the properties of these four modes. We find that self-gravity, to a certain degree, reduces their frequencies and changes the structure of the dispersion curves and eigenfunctions at radial wavelengths comparable to the disc height. Its influence on the basic branch of the r-mode, in the case of subadiabatic and adiabatic stratifications, and on the basic branch of the g-mode, in the case of superadiabatic stratification (which in addition exhibits convective instability), does appear to be strongest. Reducing the three-dimensional Toomre's parameter Q_{3D} results in the latter modes becoming unstable due to self-gravity, so that they determine the onset criterion and nature of the gravitational instability of a vertically stratified disc. By contrast, the p-, f- and convectively stable g-modes, although their corresponding ω^2 are reduced by self-gravity, never become unstable however small the value of Q_{3D} . This is a consequence of the three-dimensionality of the disc. The eigenfunctions corresponding to the gravitationally unstable modes are intrinsically three-dimensional. We also contrast the more exact instability criterion based on our three-dimensional model with that of density waves in two-dimensional (razor-thin) discs. Based on these findings, we comment on the origin of surface distortions seen in numerical simulations of self-gravitating discs.

Key words: accretion, accretion discs – gravitation – hydrodynamics – instabilities – convection – (stars:)planetary systems: protoplanetary discs – turbulence

1 INTRODUCTION

Self-gravity plays an important role in a variety of astrophysical systems. It is a main agent determining the dynamical evolution of star clusters, galaxies, various types of accretion discs, etc. Particularly in protoplanetary discs, that are the central subject of our study, self-gravity provides one of the main source of outward angular momentum transport through the excitation of density waves (Papaloizou & Savonije 1991; Laughlin & Bodenheimer 1994; Lodato & Rice 2004, 2005) and is able to cause fragmentation of a disc into bound clumps, or planets, under

certain conditions (Gammie 2001; Rice et al. 2003, 2005; Boss 2004; Mayer et al. 2007; Rafikov 2007). Starting with the seminal paper by Toomre (1964), there have been a large number of studies of the stability of self-gravitating gaseous discs, both in the linear (e.g., Goldreich & Lynden-Bell 1965a,b; Goldreich & Tremaine 1978; Adams et al. 1989; Bertin et al. 1989; Papaloizou & Lin 1989; Laughlin et al. 1997) and non-linear regimes, including other relevant physical factors (e.g., heating, cooling, radiation transport) with up-to-date numerical techniques (e.g., Papaloizou & Savonije 1991; Laughlin & Bodenheimer 1994; Boss 1998; Pickett et al. 2000, 2003; Gammie 2001; Boss 2003; Johnson & Gammie 2003; Rice et al. 2003, 2005;

* E-mail: grm@roe.ac.uk

Boss 2004; Mejía et al. 2005; Boley et al. 2006; Mayer et al. 2007; Stamatellos & Whitworth 2009).

Linear stability analysis in a vast majority of cases is restricted, for simplicity, to razor-thin, or two-dimensional (2D) discs that are obtained by vertically averaging all quantities. In other words, perturbations are assumed to have large horizontal scales compared with the disc thickness. In this limit, the well-known Toomre's parameter

$$Q_{2D} = \frac{c_s \Omega}{\pi G \Sigma}$$

controls the stability of self-gravitating discs (Toomre 1964). In this case, a density wave, which is the only mode in a 2D disc, is influenced by self-gravity and thus can become unstable, as the local dispersion relation for the latter clearly demonstrates (Goldreich & Tremaine 1978; Binney & Tremaine 1987; Bertin et al. 1989).

Stability analysis in a more realistic case of self-gravitating three-dimensional (3D) discs is more complicated. The disc is vertically stratified due to both its own self-gravity and the vertical component of the gravity of a central object. Depending on the nature of the stratification, there exists a whole new set of various vertical modes in the system (see below), some of which can become unstable due to self-gravity on horizontal length scales comparable to the disc thickness. In this situation, the vertical variation of perturbations is important and for a correct characterization of the gravitational instability it is necessary to introduce another parameter not involving height-dependent variables, such as the sound speed in Toomre's parameter. Furthermore, not all types of stratification permit two-dimensional modes, that is, modes with no vertical motions commonly occurring in the 2D treatment. For example, in non-self-gravitating discs with polytropic vertical structure, there are no 2D modes (Lin et al. 1990; Lubow & Pringle 1993b; Korycansky & Pringle 1995) implying that the dynamics does not always reduce to that of the 2D case. Therefore, a more accurate stability analysis of self-gravitating discs should necessarily be three-dimensional.

Obviously, before studying the gravitational instability of stratified discs, one must first classify and characterize vertical normal modes of perturbations in the simplified case of no self-gravity. Analysis of the modal structure of stratified, polytropic, compressible, non-self-gravitating discs has been done in several papers: Ruden et al. (1988, hereafter RPL), Korycansky & Pringle (1995, hereafter KP), Ogilvie (1998). In convectively stable discs, i.e., with subadiabatic vertical stratification, four principal types of vertical modes can be distinguished. These modes are: acoustic p-modes, surface gravity f-modes, buoyancy g-modes and inertial r-modes. The modes are named after their corresponding restoring forces, which can be well identified for each mode at horizontal wavelengths smaller than the disc height and are provided by one of the following: compressibility/pressure, displacements of free surfaces of a disc, buoyancy due to vertical stratification and inertial forces due to disc rotation, respectively, for the p-, f-, g- and r-modes. In the case of superadiabatic stratification, the r- and g-modes merge and appear as a single mode, which becomes convectively unstable for horizontal wavenumbers larger than a certain value (RPL); the p- and f-modes remain qualitatively unchanged. For neutral/adiabatic stratification, buoy-

ancy is absent and the g-mode disappears. *The main purpose of this paper is to investigate how self-gravity modifies the frequencies and the structure of the eigenfunctions of these modes, which mode acquires the largest positive growth rate due to self-gravity and, therefore, determines the onset criterion and nature of the gravitational instability of a stratified disc.* So, the mode dynamics in the 3D case can appear more complex than that in the 2D one, where only the density wave mode can be subject to gravitational instability. Previously, Goldreich & Lynden-Bell (1965a, hereafter GLB) considered gravitational instability in a uniformly rotating gaseous slab with an adiabatic vertical stratification, thereby leaving out all modes associated with buoyancy. Other studies also considered the gravitational instability of 3D galactic discs, however, the analysis was essentially 2D, finite-thickness effects were only taken into account by means of various reduction factors in 2D dispersion relations (Shu 1968; Romeo 1992, 1994). In all these studies, as in GLB, the main focus was on finding the criterion for the onset of gravitational instability, so that a full analysis of various types of vertical normal modes existing in stratified self-gravitating discs was not carried out. Actually, we generalize the study of GLB to subadiabatic and superadiabatic stratifications having different modal structure.

Another motivation for our study is that the f-mode is thought to play an important dynamical role in self-gravitating discs. The non-linear behaviour of 3D perturbations involving large surface distortions, as seen in numerical simulations, has been attributed to the surface gravity f-mode (Pickett et al. 2000). However, this was done without analysing the behaviour of other vertical modes under self-gravity. It was shown that the f-mode leads to a large energy dissipation in the vicinity of the disc surface, which may facilitate disc cooling, because the energy is deposited at smaller optical depth where it can be radiated away more quickly (see e.g., Johnson & Gammie 2003; Boley et al. 2006). Later it was realized that in fact the non-linear vertical motions in self-gravitating discs can be much more complex than just the f-mode and can have a shock character (shock bores, Boley & Durisen 2006). Thus, in the 3D case, the dynamics of self-gravitating discs is much richer and diverse than that of idealized 2D ones and requires further study. To fully understand the origin of such three-dimensional effects and what type of instability they are associated with, one should start with a rigorous linear study of the characteristic properties of all the types of vertical normal modes mentioned above, not only the f-mode, in the presence of self-gravity. The present work is just a first step in this direction.

Numerical simulations of self-gravitating discs are often in the context of global discs (e.g., Pickett et al. 2000, 2003; Rice et al. 2003, 2005; Lodato & Rice 2004, 2005; Boley et al. 2006; Boley 2009) and, therefore, are not always able to well resolve vertical motions, which, as shown in the present study, inevitably arise during the development of the gravitational instability associated with intrinsically three-dimensional modes. So, these simulations may not quite accurately capture all the subtleties of the gravitational instability in 3D discs. In this connection, we should mention the work by Nelson (2006) that extensively discusses the issue of vertical resolution and its importance in the outcome of the gravitational instability in numerical

simulations of self-gravitation discs. Resolving and analysing vertical motions are also crucial for properly understanding cooling processes in discs and, particularly, whether convection is able to provide sufficiently effective cooling for disc fragmentation to occur, which is still a matter for debate in the literature (Boss 2004; Mayer et al. 2007; Boley et al. 2006, 2007; Rafikov 2007). In addition, these studies, for simplicity, use the criterion for gravitational instability based on the two-dimensional Toomre's parameter, which, as we will demonstrate, cannot always be uniquely mapped into an analogous three-dimensional stability parameter and give a precise criterion for the onset of gravitational instability.

In this paper, following other works in a similar vein: Lubow & Pringle (1993b, hereafter LP), KP, Lubow & Ogilvie (1998, hereafter LO98), we adopt the shearing box approximation and consider the linear dynamics of vertical normal modes of perturbations in a compressible, stratified, self-gravitating gaseous disc with Keplerian rotation. In the unperturbed disc, pressure and density are related by a polytropic law, which is a reasonably good approximation for optically thick discs (see e.g., LO98). This allows us to consider the specific features of the dynamics for subadiabatic, adiabatic and superadiabatic vertical stratifications by simply varying the polytropic index. As a first step towards understanding the effects of self-gravity on the perturbation modes, we restrict ourselves to axisymmetric perturbations only. The linear results obtained here will form the basis for studying the non-linear development of gravitational instability in the local shearing box approximation that allows much higher numerical resolution than global disc models can afford.

The paper is organized as follows. The physical model and basic equations are introduced in Section 2. The classification of vertical modes in the absence of self-gravity is performed in Section 3. Effects of self-gravity on all normal modes are analysed in Section 4. In Section 5, we focus on the properties of gravitational instability in 3D. Comparison between the criteria of gravitational instability in 3D and 2D is made in Section 6. Summary and discussions are given in Section 7.

2 PHYSICAL MODEL AND EQUATIONS

In order to study the dynamics of three-dimensional modes in gaseous self-gravitating discs, following LP, KP, LO98, we adopt a local shearing box approximation (Goldreich & Lynden-Bell 1965b). In the shearing box model, the disc dynamics is studied in a local Cartesian reference frame rotating with the angular velocity of disc rotation at some fiducial radius from the central star, so that curvature effects due to cylindrical geometry of the disc are ignored. In this coordinate frame, the unperturbed differential rotation of the disc manifests itself as a parallel azimuthal flow with a constant velocity shear in the radial direction. A Coriolis force is included to take into account the effects of coordinate frame rotation. The vertical component of the gravity force of the central object is also present. As a result, we can write down the three-dimensional shearing box equations

$$\frac{d\mathbf{u}}{dt} + 2\Omega\hat{\mathbf{z}} \times \mathbf{u} + \nabla \left(-q\Omega^2 x^2 + \frac{1}{2}\Omega^2 z^2 + \psi \right) + \frac{1}{\rho}\nabla p = 0, \quad (1)$$

$$\frac{d\rho}{dt} + \rho\nabla \cdot \mathbf{u} = 0 \quad (2)$$

and the equation of conservation of entropy

$$\frac{d}{dt} \left(\frac{p}{\rho^\gamma} \right) = 0. \quad (3)$$

This set of equations is supplemented with Poisson's equation to take care of disc self-gravity

$$\left(\frac{\partial^2}{\partial x^2} + \frac{\partial^2}{\partial y^2} + \frac{\partial^2}{\partial z^2} \right) \psi = 4\pi G\rho. \quad (4)$$

Here $\mathbf{u} = (u_x, u_y, u_z)$ is the velocity in the local frame, p, ρ, ψ are, respectively, the pressure, density and the gravitational potential of the disc gas. Ω is the angular velocity of the local reference frame rotation as a whole, x, y, z are, respectively, the radial, azimuthal and vertical coordinates, $\hat{\mathbf{z}}$ is the unit vector along the vertical direction and $d/dt = \partial/\partial t + \mathbf{u} \cdot \nabla$ is the total time derivative. The shear parameter is $q = 1.5$ for the Keplerian rotation considered in this paper. The adiabatic index, or the ratio of specific heats, $\gamma = 1.4$ as typical of a disc composed of molecular hydrogen; we adopt this value throughout the paper.

2.1 The equilibrium disc model

Equations (1-4) have an equilibrium solution that is stationary and axisymmetric. In this unperturbed state, the velocity field represents, as noted above, a parallel azimuthal flow, \mathbf{u}_0 , with a constant radial shear q :

$$u_{x0} = u_{z0} = 0, \quad u_{y0} = -q\Omega x.$$

In the shearing box, the equilibrium density ρ_0 , pressure p_0 and gravitational potential ψ_0 depend only on the vertical z -coordinate and satisfy the hydrostatic relation

$$g_0 \equiv -\frac{1}{\rho_0} \frac{dp_0}{dz} = \Omega^2 z + \frac{d\psi_0}{dz}, \quad (5)$$

$$\frac{d^2\psi_0}{dz^2} = 4\pi G\rho_0. \quad (6)$$

As in LP, KP and RPL, pressure and density in the unperturbed disc are related by a polytropic relationship of the form

$$p_0 = K\rho_0^{1+1/s}, \quad (7)$$

where K is the polytropic constant and $s > 0$ is the polytropic index. The Brunt-Väisälä frequency squared is defined as

$$N_0^2 \equiv \frac{g_0}{\rho_0} \left(\frac{1}{c_s^2} \frac{dp_0}{dz} - \frac{d\rho_0}{dz} \right) = \left(\frac{\gamma s}{s+1} - 1 \right) \frac{g_0^2}{c_s^2}, \quad (8)$$

where $c_s^2 = \gamma p_0/\rho_0$ is the adiabatic sound speed squared. If $1 + 1/s < \gamma$ (subadiabatic thermal stratification), then $N_0^2 > 0$ all along the height and the equilibrium vertical structure of the disc is convectively stable. In the opposite case $1 + 1/s > \gamma$ (superadiabatic thermal stratification), $N_0^2 < 0$ everywhere and this corresponds to a convectively unstable equilibrium. For $1 + 1/s = \gamma$ (adiabatic thermal stratification), $N_0^2 = 0$ and all the motions/modes due to buoyancy disappear. Later we will consider these three regimes separately.

To determine the vertical structure, we need to solve equations (5-6) subject to the boundary condition that the pressure vanish at the free surface of the disc. Because we have a polytropic model, it is convenient to work with the pseudo-enthalpy

$$w_0 = (s + 1)K\rho_0^{1/s}.$$

The disc structure is also symmetric with respect to the mid-plane, $z = 0$, and, as a consequence, it follows from equations (5-7) that the derivative of w_0 at the midplane vanishes (i.e., $dw_0/dz(0) = 0$). Because of this reflection symmetry, we consider only the upper half of the disc, $z \geq 0$. At the surface of the disc $w_0 = 0$, similar to the pressure. This allows us to determine the equilibrium vertical structure of the disc. The non-dimensional variables being used throughout the paper are:

$$\begin{aligned} x &\rightarrow \frac{x\Omega}{c_{sm}}, & y &\rightarrow \frac{y\Omega}{c_{sm}}, & z &\rightarrow \frac{z\Omega}{c_{sm}}, \\ \rho_0 &\rightarrow \frac{\rho_0}{\rho_m}, & w_0 &\rightarrow \frac{w_0}{w_m}, & c_s &\rightarrow \frac{c_s}{c_{sm}}, \end{aligned}$$

where $\rho_m \equiv \rho_0(0)$, $w_m \equiv w_0(0)$, $c_{sm} \equiv c_s(0)$ are the mid-plane values of the equilibrium density, pseudo-enthalpy and sound speed. We define the three-dimensional analogue of Toomre's parameter as

$$Q_{3D} = \frac{\Omega^2}{4\pi G \rho_m},$$

which is a measure of disc self-gravity (from now on until Section 6, we will use Q_{3D} without subscript everywhere, so it should not be confused with the 2D Toomre's parameter). Using that at the midplane $dw_0/dz(0) = 0$, we can derive from equations (5-7) a single equation for the normalized pseudo-enthalpy

$$\frac{s+1}{2\gamma} \left(\frac{dw_0}{dz} \right)^2 = (1 - w_0) + \frac{1}{Q(s+1)}(1 - w_0^{s+1}). \quad (9)$$

The normalized density and sound speed are found from $\rho_0 = w_0^s$, $c_s^2 = w_0$. Equation (9) shows that even though the disc is in Keplerian rotation (i.e., self-gravity in the radial direction can be neglected), it must be included in determining the vertical structure. We integrate equation (9), starting at $z = 0$ with $w_0(0) = 1$, until w_0 , monotonically decreasing with z , reaches zero at some finite height/edge $z = h$, which is therefore determined as a result of the integration process. At this edge, the density and sound speed also vanish, $\rho_0(h) = 0$, $c_s(h) = 0$ (see also GLB and RPL). The height and entire vertical structure of a polytropic disc are therefore uniquely specified solely by Q and s , which are free parameters in equation (9).

Figure 1 illustrates the sub- and superadiabatic equilibrium vertical structures obtained from equation (9) for various Q . For a fixed s , the disc height h decreases with decreasing Q . The sound speed is a decreasing function of z that does not permit the existence of two-dimensional modes in three-dimensional models of polytropic discs as opposed to isothermal ones (Lin et al. 1990, LP, KP). We also see that the equilibrium structures for sub- and superadiabatic cases look similar except that they have, respectively, everywhere positive and negative N_0^2 that diverges at the surface because the sound speed vanishes there.

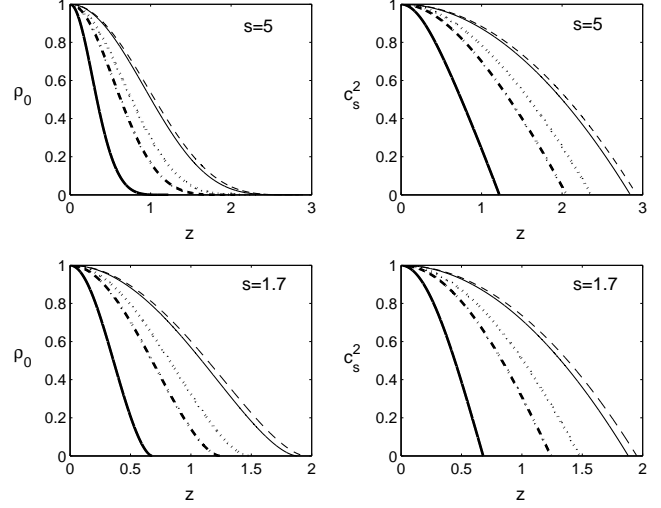


Figure 1. Vertical variations of the normalized density and squared sound speed for subadiabatic ($s = 5$) and superadiabatic ($s = 1.7$) equilibrium states with $Q = 0.1$ (thick solid lines), $Q = 0.5$ (dashed-dotted lines), $Q = 1$ (dotted lines), $Q = 10$ (thin solid lines) and the non-self-gravitating case ($Q \rightarrow \infty$, dashed lines). The lines corresponding to $Q = 10$ are close to those in the non-self-gravitating limit, implying that the role of self-gravity is negligible for $Q \geq 10$. The disc heights, h , are different depending on Q and s .

2.2 Perturbation equations

We consider here small axisymmetric ($\partial/\partial y = 0$) perturbations of the form $\mathbf{u}', \rho', p', \psi' \propto \exp(-i\omega t + ikx)$ about the equilibrium states found above, where ω and k are the frequency and the radial wavenumber, respectively. Without a loss of generality, we assume throughout that k is non-negative, $k \geq 0$. After switching to non-dimensional variables:

$$t \rightarrow \Omega t, \quad \omega \rightarrow \frac{\omega}{\Omega},$$

$$k \rightarrow \frac{kc_{sm}}{\Omega}, \quad N_0 \rightarrow \frac{N_0}{\Omega}, \quad g_0 \rightarrow \frac{g_0}{\Omega c_{sm}},$$

$$u'_x \rightarrow \frac{u'_x}{c_{sm}}, \quad u'_y \rightarrow \frac{u'_y}{c_{sm}}, \quad u'_z \rightarrow \frac{u'_z}{c_{sm}},$$

$$\rho' \rightarrow \frac{\rho'}{\rho_m}, \quad p' \rightarrow \frac{p'}{\rho_m c_{sm}^2}, \quad \psi' \rightarrow \frac{\psi'}{c_{sm}^2},$$

we can derive from equations (1-4) the following set of equations governing the linear dynamics of axisymmetric perturbations

$$-i\omega u'_x = -\frac{ikp'}{\rho_0} + 2u'_y - ik\psi' \quad (10)$$

$$-i\omega u'_y = (q - 2)u'_x \quad (11)$$

$$-i\omega u'_z = -\frac{1}{\rho_0} \frac{dp'}{dz} - g_0 \frac{\rho'}{\rho_0} - \frac{d\psi'}{dz} \quad (12)$$

$$-i\omega \rho' + ik\rho_0 u'_x + \frac{d}{dz}(\rho_0 u'_z) = 0 \quad (13)$$

$$-i\omega(p' - c_s^2 \rho') + \frac{\rho_0 c_s^2 N_0^2}{g_0} u'_z = 0 \quad (14)$$

$$\left(-k^2 + \frac{d^2}{dz^2}\right)\psi' = \frac{\rho'}{Q}. \quad (15)$$

If we now make the changes: $iu'_z \rightarrow u'_z$, $\omega p'/\rho_0 \rightarrow p'$, $\omega\psi' \rightarrow \psi'$ and eliminate u'_x , u'_y , ρ' from equations (10), (11), (13), we arrive at the following set of equations for the three basic quantities u'_z , p' , ψ' (henceforth primes will be omitted)

$$\frac{du_z}{dz} = \frac{g_0}{c_s^2}u_z - \left(\frac{1}{c_s^2} - \frac{k^2}{\omega^2 - \kappa^2}\right)p + \frac{k^2\psi}{\omega^2 - \kappa^2} \quad (16)$$

$$\frac{dp}{dz} = \frac{N_0^2}{g_0}p + (\omega^2 - N_0^2)u_z - \frac{d\psi}{dz} \quad (17)$$

$$\frac{d^2\psi}{dz^2} - k^2\psi = \frac{\rho_0}{Q}\left(\frac{p}{c_s^2} + \frac{N_0^2}{g_0}u_z\right), \quad (18)$$

where the non-dimensional epicyclic frequency κ is given by $\kappa^2 = 2(2 - q) = 1$. Notice that the density perturbations on the right hand side of the linearized Poisson's equation (18) consist of two physically different parts. The density perturbations due to compressibility, which are inversely proportional to the squared sound speed and proportional to the pressure perturbation, and the density perturbations due to the stratified background, which are proportional to the vertical velocity perturbation and N_0^2 . This latter term due to stratification is obviously absent in the two-dimensional analysis of gravitational instability as well as when the disc is adiabatic (see GLB). Equations (16-18) form the basis for determining the axisymmetric normal modes of perturbations existing in compressible, stratified, polytropic, self-gravitating discs. In the non-self-gravitating limit, these equations reduce to the main equations of KP. The reflection symmetry of the unperturbed disc allows us to take the eigenfunctions/modes to be either even or odd with respect to z . So, to determine the eigenfrequencies (dispersion diagrams, that is, ω as a function of k for various branches) and eigenfunctions, we can numerically integrate the main equations (16-18) only in the upper half, $0 \leq z \leq h$, of the full vertical extent of the disc provided that suitable boundary conditions are imposed at $z = 0$ and $z = h$. In other words, we need to solve a boundary value problem. Here the disc height h , as noted above, is determined by the parameters Q and s . By inspecting equations (16-18), it is clear that a normal mode whose pressure p and potential ψ perturbations are even functions under reflection in z , has odd vertical velocity u_z and gravitational potential derivative $d\psi/dz$ perturbations under reflection and vice versa. We define a normal mode as being 'even' ('odd') if the corresponding vertical velocity and gravitational potential derivative are odd (even) functions of z (this convention agrees with that of Ogilvie 1998, but differs from LP and KP). Thus, the boundary conditions at the midplane, $z = 0$, for the even modes are:

$$u_z(0) = 0, \quad d\psi/dz(0) = 0 \quad (19)$$

and for the odd modes are:

$$p(0) = 0, \quad \psi(0) = 0. \quad (20)$$

At $z = h$ we impose the usual free-surface boundary condition for which the Lagrangian pressure perturbation vanishes. In our new non-dimensional variables this translates as

$$p = g_0 u_z \quad \text{at} \quad z = h. \quad (21)$$

The boundary condition for the gravitational potential can be derived by treating the surface displacement as a surface distribution of gravitating matter at $z = h$. Using the continuity of potential across the boundary, Gauss's flux theorem and the fact that outside the disc, at $z \rightarrow \pm\infty$, gravitational potential should vanish, we arrive at the following condition at the disc surface (see e.g., GLB, Lubow & Pringle 1993a)

$$\frac{d\psi}{dz} + k\psi = -\frac{u_z \rho_0}{Q} \quad \text{at} \quad z = h. \quad (22)$$

Equations (16-18) supplemented with boundary conditions (21),(22) at the surface $z = h$ and (19),(20) at the midplane fully determine a boundary value problem. Using these boundary conditions and variational principle, it can be easily shown that ω^2 is real (GLB, RPL) that much alleviates the search of eigenfrequencies. We integrate these equations from $z = h$ downwards to $z = 0$ separately for the even modes under conditions (19) and for the odd modes under conditions (20). We will see below that in the presence of self-gravity, the dispersion diagrams for these two mode parities are quite different. In other words, self-gravity influences even and odd modes, or changes their dispersion characteristics, in different ways. As is typical, for a given equilibrium structure, that is, for given Q and s , and for a given radial wavenumber k , midplane boundary conditions can be satisfied only for certain values of ω , yielding dispersion relations $\omega(k)$ for different branches of modes classified below. We use a Runge-Kutta integrator and root-finding algorithms of MATLAB package to first numerically solve differential equations (16-18) and then find eigenfrequencies.

3 THE CLASSIFICATION OF VERTICAL MODES

In this section, we for the moment remove self-gravity (put $\psi \rightarrow 0, Q \rightarrow \infty$) from the perturbation equations (16-18) and from the equilibrium in order to classify and characterize all the vertical axisymmetric normal modes existing in a three-dimensional disc. In special cases, an analogous classification of modes in non-self-gravitating discs has been done previously by several authors (RPL, LP, KP, Ogilvie 1998). The aim here is to briefly review and synthesize the results from these studies. In the next section, we will again switch on self-gravity and investigate how it affects the characteristics of these modes. Accordingly, in the non-self-gravitating case, we need the midplane and surface boundary conditions discussed above, but only for pressure and vertical velocity perturbations.

Figure 2 shows the typical dispersion diagrams for three types of equilibria: subadiabatic ($1 + 1/s < \gamma$), adiabatic ($1 + 1/s = \gamma$) and superadiabatic ($1 + 1/s > \gamma$) stratifications. In the subadiabatic case, one can identify four distinct classes of vertical normal modes (see also KP, Ogilvie 1998). These modes are: the acoustic p-modes, the surface gravity f-modes, the buoyancy g-modes and the inertial r-modes the restoring forces for which at large radial wavenumbers $kh \gg 1$ are mainly provided, respectively, by compressibility/pressure, by the displacements of free surface of the disc, by buoyancy due to the vertical entropy gradient and by

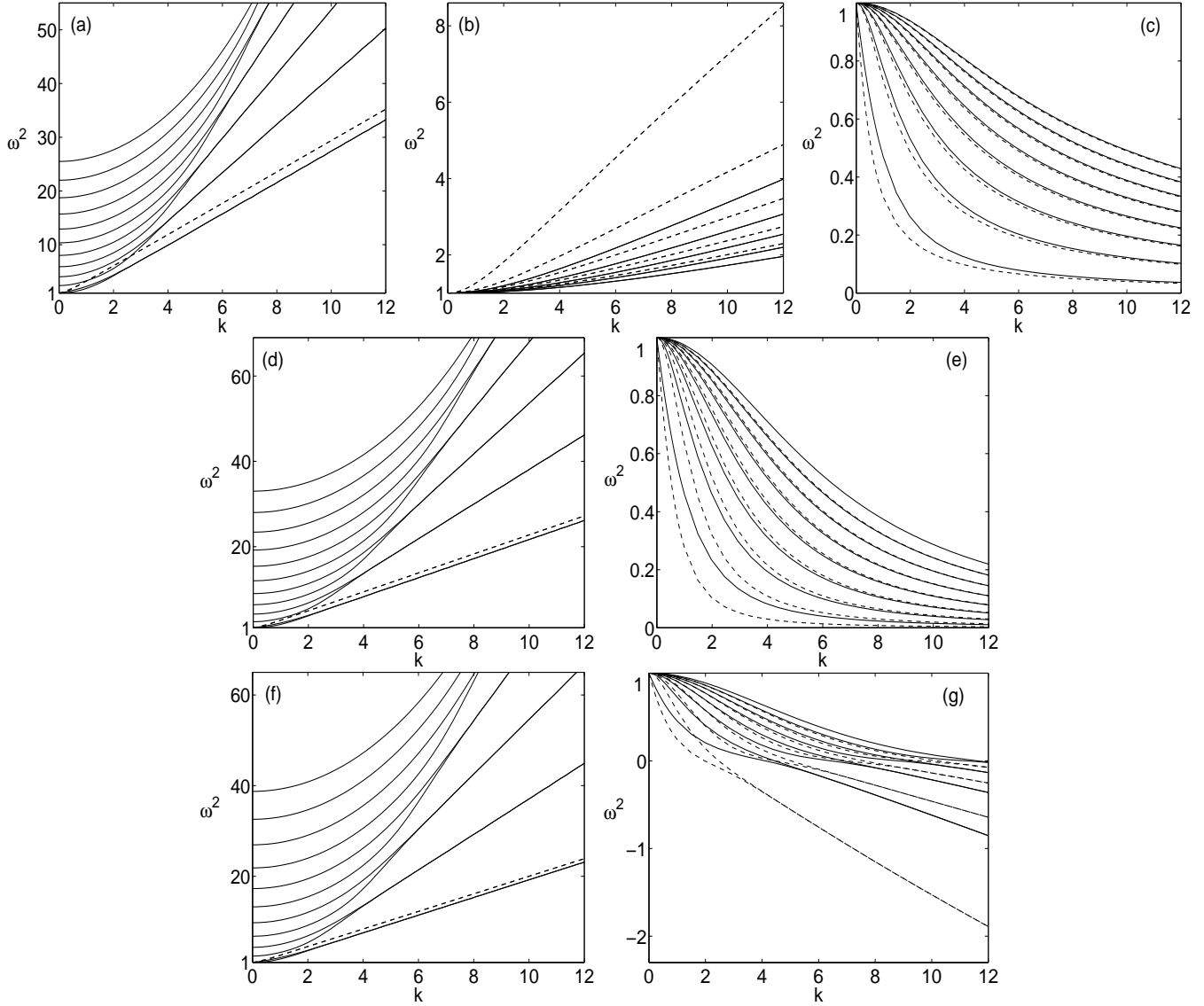


Figure 2. Dispersion diagrams in the non-self-gravitating case for a subadiabatic disc with $s = 5$ (panels a, b, c), for an adiabatic disc with $s = 2.5$ (panels d, e) and for a superadiabatic disc with $s = 1.7$ (panels f, g). The solid lines in panels (a), (d), (f) show the frequencies for different branches of the surface gravity f- and acoustic p-modes vs. radial wavenumber k . In order of increasing frequency these branches/curves are $f_0^e, f_0^o, p_1^e, p_1^o, p_2^e, p_2^o, p_3^e, p_3^o, p_4^e, p_4^o, p_5^e, p_5^o$ (superscripts denote the even and odd modes, which are numbered, respectively, according to the number of nodes of vertical velocity and pressure perturbations in the interval $0 < z \leq h$). Although, for large k , the frequencies of even and odd modes coalesce. The dashed lines in these panels correspond to frequencies of the f-modes computed in the incompressible limit. The solid lines in panel (b) show the convectively stable g-mode branches, which in order of decreasing frequency are $g_1^{o,e}, g_2^{o,e}, g_3^{o,e}, g_4^{o,e}, g_5^{o,e}$. Here the frequencies of even and odd modes coincide. The solid lines in panels (c), (e) show the r-mode branches, which in order of increasing frequency are $r_0^e, r_0^o, r_1^e, r_1^o, r_2^e, r_2^o, r_3^e, r_3^o$ (r_0^e and r_0^o are the basic even and odd r-modes and subscript ‘0’ means that, respectively, vertical velocity and pressure perturbations for them have no nodes in the interval $0 < z \leq h$). In this respect, our numbering of modes differs from that of Ogilvie 1998). The solid lines in panel (g) show the convectively unstable g-modes, which in order of increasing ω^2 are $g_0^e, g_0^o, g_1^e, g_1^o, g_2^e, g_2^o, g_3^e, g_3^o$ (g_0^e denotes the basic even g-mode, the corresponding vertical velocity perturbation for which has no nodes in the range $0 < z \leq h$). Similar to the p-modes, the convectively unstable even and odd g-modes coalesce at large k . In each panel, the dashed lines show the corresponding mode branches computed for the incompressible case with the same ordering of eigenfrequencies. From panels (b), (g), we see that compressibility most strongly affects the convectively stable and unstable g-modes.

inertial forces due to disc rotation. The existence of the g-modes in polytropic discs is attributable to the variation of the sound speed and N_0 with height; the latter diverges at the disc surface giving rise to the trapped g-mode there. For $1 + 1/s < \gamma$, all these modes have $\omega^2 > 0$ and, therefore, are stable. The p-, f- and g-modes are high-frequency modes

with frequencies always larger than the epicyclic frequency, $\omega^2 \geq \kappa^2$, while the r-mode is of low-frequency with $\omega^2 \leq \kappa^2$ (we remind that hereafter $\kappa = 1$).

For adiabatic stratification, there is no buoyancy ($N_0^2 = 0$) and, therefore the g-mode disappears, while other modes remain qualitatively unchanged. Similarly, the r-mode does

not exist in a disc that has zero epicyclic frequency. For $1 + 1/s > \gamma$, the g-mode becomes convectively unstable ($\omega^2 < 0$) for radial wavenumbers larger than a certain value because of negative buoyancy. Its characteristic timescale (growth rate) can be of the order of the epicyclic frequency or less and due to this, it interferes with motions corresponding to the r-mode. Consequently, in the superadiabatic case, the r- and g-modes merge at $\omega^2 \leq \kappa^2$ and appear as a single mode, which we still call the g-mode and not the r-mode, because the behaviour of corresponding eigenfunctions with height in this case is similar to that of the convectively stable g-mode (see also RPL); the p- and f-modes are not much affected.

All these modes come in even and odd pairs. In Fig. 2, even (odd) modes are numbered according to the number of nodes of the vertical velocity (pressure) perturbation in the interval $0 < z \leq h$ (the node at $z = 0$ is not counted). We also see the coalescence of the dispersion curves of the even and odd p- and f-modes and also the convectively unstable even and odd g-modes as k increases past a certain point, which depends on the mode number (RPL, KP). This is associated with a transition from oscillatory to evanescent behaviour of eigenfunctions. We do not plot eigenfunctions here, as an extensive discussion of their properties can be found in RPL, KP, LO98 and Ogilvie (1998). We only mention that the eigenfunctions of the p- and g-modes are trapped near the surfaces and decay towards the midplane, while the eigenfunctions of the r-mode are concentrated near the midplane and decay towards the surfaces. As for the eigenfunctions of the fundamental f-mode, they have no nodes and monotonically decay from the surfaces to the midplane. Below we show that these properties of eigenfunctions are altered due to self-gravity. Specifically, the number of nodes along each branch of the dispersion diagrams, which is preserved in the non-self-gravitating limit, is no longer constant in the presence of self-gravity. The frequencies of the p- and r-modes increase with mode number. The frequencies and growth rates of the convectively stable and unstable g-modes, respectively, decrease with the mode number. These are the well-known general properties of vertical modes in polytropic discs.

Although each mode type has its dominant restoring force, one out of the above mentioned four types (compressibility, surface gravity, buoyancy, inertial forces), the other three forces also contribute to a certain degree for small radial wavenumbers $kh \lesssim 1$. For example, the p- and f-modes are modified both by rotation/inertial forces and buoyancy, the f-mode is also modified by compressibility, the g-mode is modified by rotation and compressibility and the r-mode is modified by buoyancy and compressibility. For the sake of comparison with the relevant result from previous studies, we are particularly interested in to what degree compressibility modifies generally non-compressive f-, g- and r-modes. So, we decided to juxtapose the dispersion diagrams for these modes computed separately in the compressible and incompressible cases. We take the incompressible limit by formally letting the adiabatic index go to infinity, $\gamma \rightarrow \infty$ (Ogilvie 1998). After that equations (16-18) without self-gravity take the form

$$\frac{du_z}{dz} = \frac{k^2}{\omega^2 - \kappa^2} p$$

$$\frac{dp}{dz} = \frac{N_0^2}{g_0} p + (\omega^2 - N_0^2) u_z.$$

We solved these equations with the same boundary conditions and found the dispersion diagrams of the f-, g- and r-modes that survive in this limit (obviously, the acoustic p-mode disappears). The results are plotted in Fig. 2 with dashed lines. Notice that by taking the incompressible limit in this manner, we have been able to retain the f-mode, as expected. Instead, KP set the density perturbations to zero in the linearized continuity equation (anelastic approximation) that resulted in the f-mode disappearing in their incompressible limit. We see that compressibility most strongly affects the convectively stable and unstable g-mode branches with small mode numbers (Figs. 2b, 2g), or equivalently with vertical extent comparable to the disc height, even at large radial wavenumbers (Ogilvie 1998). The frequencies of the f- and r-modes do not change much, indicating that these modes are nearly incompressible.

4 VERTICAL MODES IN THE PRESENCE OF SELF-GRAVITY

Having characterized all types of axisymmetric normal modes in a stratified disc, let us now compute the dispersion diagrams taking into account self-gravity in the perturbation equations and in the equilibrium. This will allow us to understand how the frequencies and the structure of the eigenfunctions of the above-described mode types are altered by self-gravity, which mode acquires the largest positive growth rate in the presence of self-gravity and, thus determines the onset criterion and nature of gravitational instability of a disc. In other words, we return to the boundary value problem formulated in Section 2, which is represented by equations (16-18) supplemented with boundary conditions (21),(22) at the surface and conditions (19),(20) of the even and odd symmetry of a solution at the midplane. For each Q and s , we first determine the corresponding vertical distribution of the equilibrium quantities in equations (16-18), $\rho_0, c_s^2, g_0, N_0^2$, with height as described in Section 2 and then based on this compute the normal modes.

Figures 3, 4, 5 and 6 show the typical dispersion diagrams for the p-, f-, g- and r-modes in a self-gravitating disc for subadiabatic, adiabatic and superadiabatic vertical stratifications. We separately plot the dispersion diagrams of the even and odd parities for each mode type to clearly see the influence of self-gravity on them, which, as evident from these figures, depends on the mode parity. Unlike in the non-self-gravitating limit, the number of nodes of the vertical velocity and pressure perturbations in the presence of self-gravity are not preserved along each mode branch. However, as we will see below, at large k , the influence of self-gravity on the mode dynamics is small and the dispersion diagrams merge with their non-self-gravitating counterparts (shown with dashed curves in Figs. 3, 5). So, the naming of the modes for smaller k , where the effect of self-gravity is important, is done by continuity with the large- k limit for each mode branch.

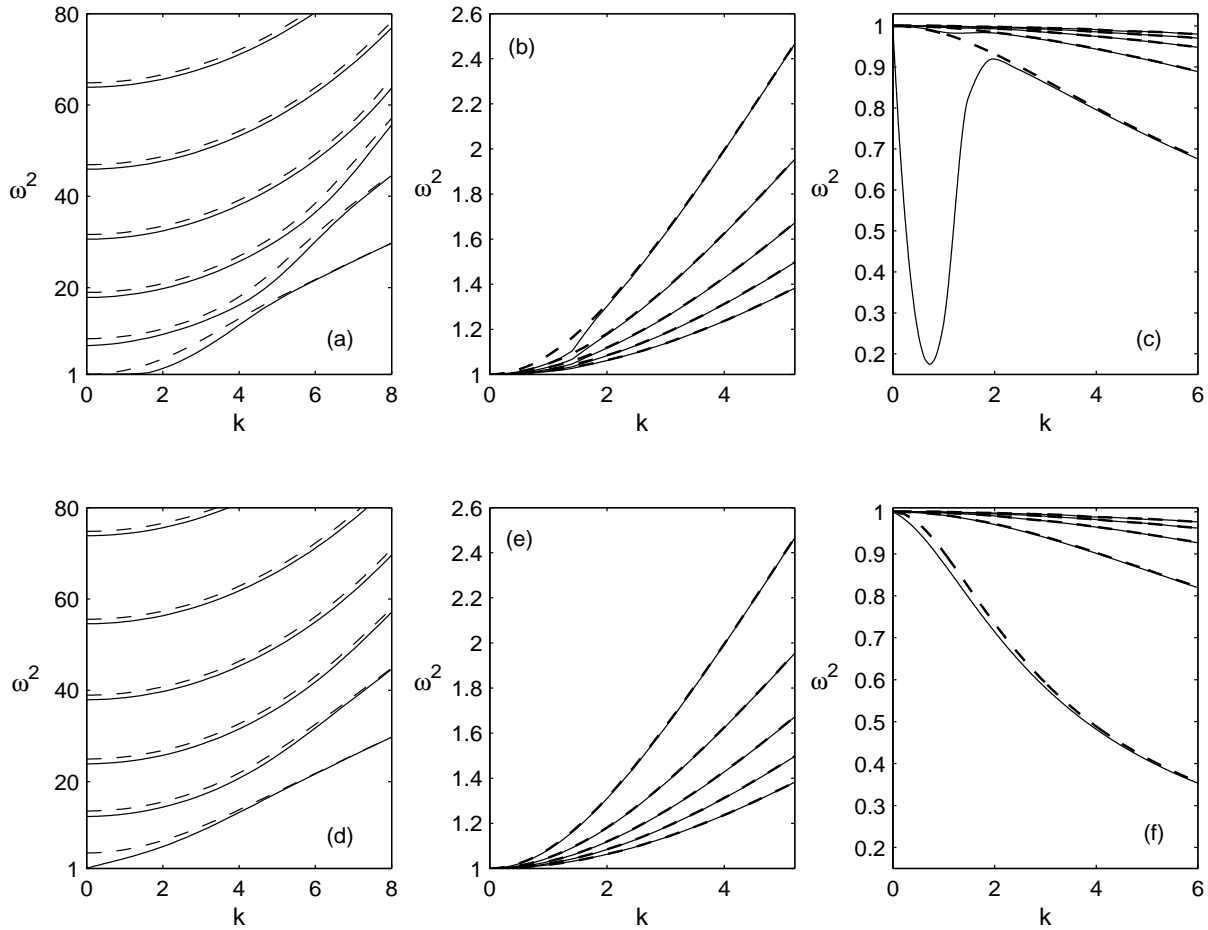


Figure 3. Dispersion diagrams of vertical modes in a subadiabatic self-gravitating disc with $s = 5$ and $Q = 0.2$. Shown are (a) the even p- and f-modes, (b) the even g-mode, (c) the even r-mode, (d) the odd p- and f-modes, (e) the odd g-mode, (f) the odd r-mode. Dashed lines are the corresponding branches computed without self-gravity in the perturbations, but with the same self-gravitating equilibrium. The frequency ordering and mode naming are the same as in Fig. 2. Self-gravity reduces/shifts the frequencies of the even and odd p-, f-modes and the even g- and r-modes mainly in the range $0 \leq k \leq 2$; the frequencies of the odd g- and r-modes are almost unaffected by self-gravity. The frequency of the basic even r-mode (denoted above as r_0^e) is modified most strongly by self-gravity as evidenced by the largest dip on the corresponding dispersion curve in panel (c). For large k and/or large mode numbers, the effect of self-gravity becomes weak and the dispersion curves merge with the dashed ones for the non-self-gravitating case.

4.1 Subadiabatic stratification

Consider first the subadiabatic case (Fig. 3), where we again have the p-, f-, g- and r-modes, but their dispersion diagrams are modified/shifted from their non-self-gravitating counterparts towards lower values due to self-gravity. As illustrated in Figs. 3a,3d, self-gravity reduces the frequencies of all branches of the p- and f-modes, for both even and odd parities, but it more affects the f-modes. The situation for the g- and r-modes is different (Figs. 3b,3c,3e,3f): only the frequencies of the even g- and r-modes are reduced by self-gravity mostly for radial wavenumbers in the range $0 \leq k \leq 2$ (dips on the corresponding dispersion curves in Figs. 3b,3c indicating deviations from the non-self-gravitating dashed ones), whereas the frequencies of the odd g- and r-modes are almost unaffected by self-gravity. The frequencies of the fundamental f-modes, the first few branches of the p-modes and also the first few branches of the even g- and r-modes are reduced noticeably. With increasing mode number and/or radial wavenumber, the effect of self-gravity on the eigenfre-

quencies gradually falls off, because the corresponding eigenfunctions become of smaller and smaller horizontal and/or vertical scale (the number of nodes increases) and take the form similar to that in the non-self-gravitating limit. As a result, the dispersion diagrams become more and more identical to their non-self-gravitating counterparts. The ordering of frequencies for the even and odd p-, f-, g- and r-modes, as it is in the non-self-gravitating case (see Fig. 2): $\omega^2(r) \leq \kappa^2 \leq \omega^2(g) < \omega^2(f) < \omega^2(p)$, is preserved in the self-gravitating case as well, however small the value of Q . Note also in Fig. 4 that the frequencies of the even and odd f-modes and also of the basic even g-mode, for which the influence of self-gravity is stronger, never fall below the epicyclic frequency with decreasing Q and, therefore, these modes always remain gravitationally stable (we also checked that the same situation holds for the dispersion curves of the even and odd f-modes in the adiabatic and superadiabatic cases described below). This is a consequence of the three-dimensionality of the disc. Thus, as evident from Figs. 3c,4d, self-gravity most significantly affects the basic branch of the

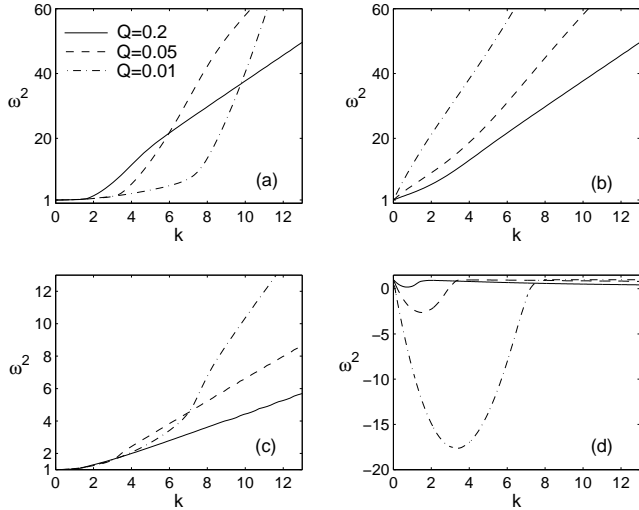


Figure 4. Dispersion curves for $s = 5$ and $Q = 0.01$ (dashed-dotted lines), $Q = 0.05$ (dashed lines), $Q = 0.2$ (solid lines). Panels (a),(b) show the even and odd f-modes, respectively. Panel (c) shows the basic even g-mode and panel (d) shows the basic even r-mode. The frequencies of the f- and g-modes never fall below the epicyclic frequency with decreasing Q and, therefore, are always stable. The basic even r-mode, which is most significantly affected by self-gravity, becomes unstable when the dip on the corresponding dispersion curve crosses the $\omega^2 = 0$ -axis. This dip deepens and broadens with decreasing Q .

even r-mode and only this branch can become unstable due to self-gravity. From Fig. 4d, it is seen that the dip on this branch deepens and broadens with decreasing Q . (We denote the wavenumber at which the minimum of this dip is located by k_m .) The gravitational instability sets in when the dip's minimum first touches the $\omega^2 = 0$ -axis at some Q_{cr} and then farther extends into the unstable $\omega^2 < 0$ region for $Q < Q_{cr}$. We will demonstrate in Section 5 that the basic even r-mode becomes strongly compressible at $k \sim k_m$ (Fig. 8), as opposed to the r-mode in a non-self-gravitating disc, and the density perturbations due to compressibility are responsible for its gravitational instability. For $s = 5$, we find $Q_{cr} = 0.168$, which gives $H = 2h = 2.96$ for the disc total thickness, and $k_m = 0.8$ (see Fig. 12). Note that the characteristic radial scale of instability $\lambda_m = 2\pi/k_m = 7.85$ is not much greater than the disc thickness H . In self-gravitating discs, compressibility and inertial forces play an important role in the dynamics of the basic even r-mode at wavelengths $\lambda \sim \lambda_m \gtrsim H$ and so it resembles a 2D density wave at such wavelengths (see Section 4.4). The fact that the characteristic scale of gravitational instability λ_m turns out to be comparable to the disc thickness may offer a clue why angular momentum transport due to self-gravity tends to be a local phenomenon (e.g., Gammie 2001; Lodato & Rice 2004; Boley et al. 2006). In this respect, it should also be mentioned that the analogous gravitational instability of low-frequency modes in a strongly compressed gaseous slab was also found by Lubow & Pringle (1993a). In their analysis, these modes, called neutral modes, are basically degenerate r-modes, since the compressed gaseous slab was not rotating.

4.2 Adiabatic stratification

In the adiabatic case (Figs. 5a-5d), there is no g-mode and the behaviour of the p-, f- and r-modes under self-gravity has qualitatively the same character as in the subadiabatic case above. Again, the basic branch of the even r-mode appears to be most significantly affected by self-gravity (the corresponding dispersion curve in Fig. 5c has the same form as that in Fig. 3c) and becomes gravitationally unstable. The ω^2 of the p- and f-modes, although lowered by self-gravity, always remain larger or equal to κ^2 irrespective of the value of Q . In this case, $s = 2.5$ and the corresponding $Q_{cr} = 0.177$ and $k_m = 0.81$. Again the radial scale of instability $\lambda_m = 2\pi/k_m = 7.75$ is not far from the disc thickness for these parameters, $H = 2h = 2.08$.

4.3 Superadiabatic stratification

The superadiabatic case (Figs. 5e-5h) is interesting, because at $\omega^2 \leq \kappa^2$, as classified above, instead of the r-mode there is the g-mode, which in addition to convective instability can also exhibit gravitational instability. As in the non-self-gravitating case, for radial wavenumbers larger than a certain value, all the branches of the g-mode become unstable because of the negative vertical entropy gradient. From Fig. 5g we see that for $0 \leq k \leq 2$, self-gravity produces dips on the g-mode dispersion curves, again preferably for the even parity ones. When Q drops sufficiently, the dip on the basic branch of the even g-mode, which appears to be most affected by self-gravity, starts to cross the $\omega^2 = 0$ -axis in a way similar to that of the basic even r-mode branch above and this signals the onset of gravitational instability. For $s = 1.7$, adopted in Fig. 5, we find $Q_{cr} = 0.184$, which gives a thickness $H = 2h = 1.76$, and $k_m = 0.83$, so that $\lambda_m = 2\pi/k_m = 7.57 \gtrsim H$. As for the p- and f-modes, they behave under self-gravity in exactly the same manner as in the above cases. In particular, although their frequencies are reduced, they can never become gravitationally unstable even for very small values of Q . Thus, for superadiabatic stratification, the basic even g-mode can exhibit two types of instabilities: gravitational and convective (see Fig. 6). As we see from Figs. 5g,6a, at moderate $Q \sim Q_{cr}$, the radial scales for the activity of self-gravity and convective instability are well separated, so that these two effects do not interfere with each other in the linear regime. For $Q = 0.1$ in Fig. 6a, self-gravity is dominant at $0 \leq k \leq 2.55$, while convective instability occurs at $k > 4.27$, where the effect of self-gravity is weak (a similar situation is for $Q = 0.2$ in Fig. 5g). However, for very small $Q \ll Q_{cr}$, the radial scales of gravitational and convective instabilities overlap (Fig. 6b), but the gas motion for such radial scales in the case of very strong gravitational instability would hardly resemble convective motions (it will look more like that in Fig. 11 below); convection is simply disrupted by gravitational instability. Therefore, we can conclude that unless a disc is strongly self-gravitating, self-gravity has little influence on the properties of convective motions and on the (Schwarzschild) criterion for the onset of convective instability that is equivalent to $N_0^2 < 0$.

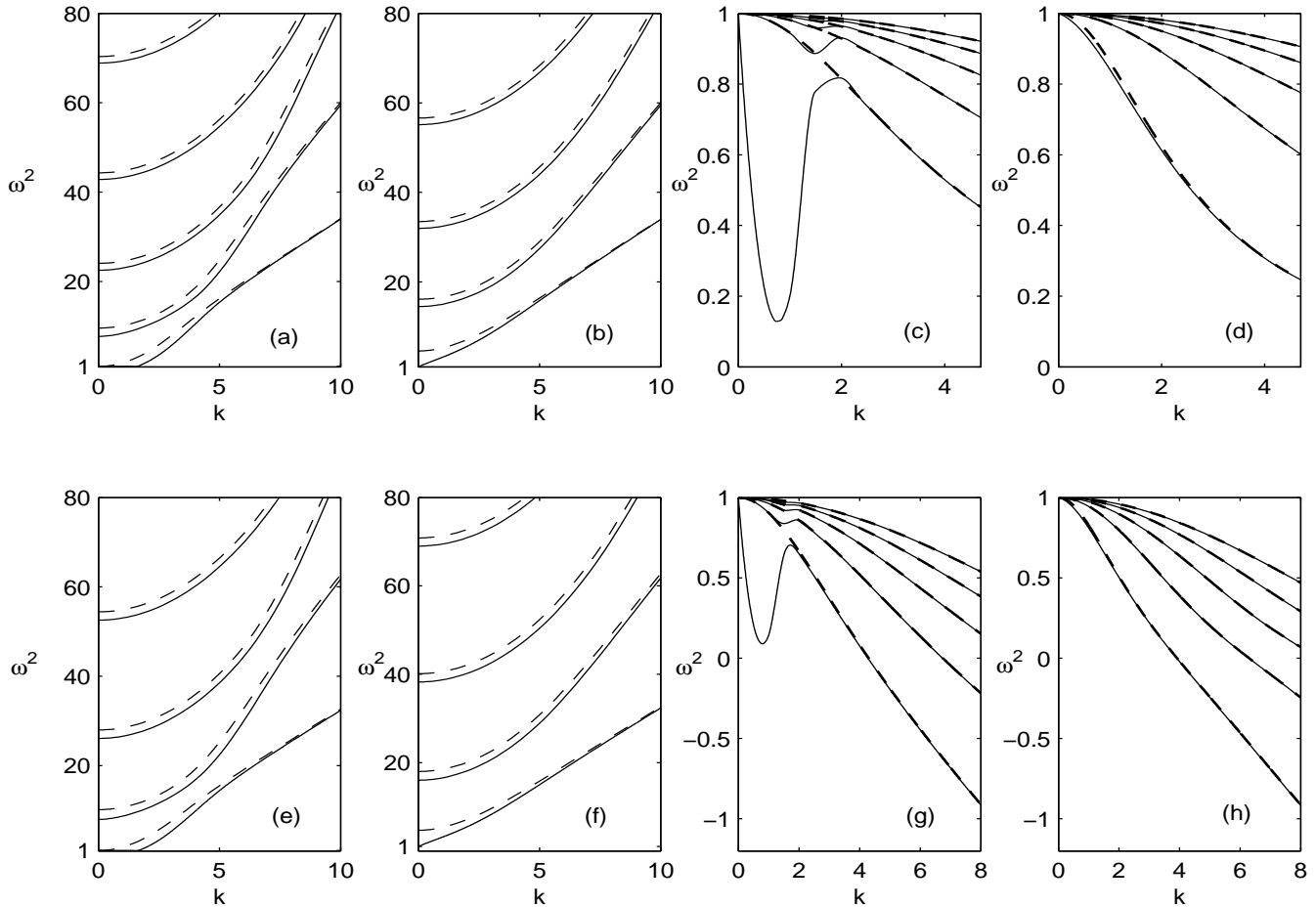


Figure 5. Dispersion diagrams for vertical modes in a self-gravitating disc with $Q = 0.2$ for an adiabatic stratification with $s = 2.5$ (panels a-d) and for a superadiabatic stratification with $s = 1.7$ (panels e-h). Shown are (a,e) the even p- and f-modes, (b,f) the odd p- and f-modes, (c) the even r-mode, (d) the odd r-mode, (g) the convectively unstable even g-mode and (h) the odd g-mode. The frequency ordering and mode naming are the same as in Fig. 2. As before, dashed curves correspond to the dispersion diagrams calculated without self-gravity in the perturbations. The behaviour of the p-, f- and r-modes in the adiabatic case is similar to that in Fig. 3. In the superadiabatic case, the dispersion curves of the even g-mode have dips caused by self-gravity in the interval $0 \leq k \leq 2$, while the odd g-mode is almost unaffected by self-gravity. The largest dip occurs for the basic branch of the even g-mode (denoted above as g_0^e) in panel (g), which appears to be most significantly influenced by self-gravity. For large k and/or large mode numbers, the effect of self-gravity becomes weak and the dispersion curves merge with dashed ones for the non-self-gravitating case. Due to the superadiabatic stratification, the even and odd g-modes are convectively unstable (i.e., have $\omega^2 < 0$) in the range $k > 3.91$, where the influence of self-gravity is small.

4.4 Analogy with the 2D density wave theory

From the three cases considered above, we conclude that the basic branch of the low-frequency ($\omega^2 \leq \kappa^2$) even mode, which is the r-mode, in the case of subadiabatic and adiabatic stratifications, and the g-mode, in the case of superadiabatic stratification, is most subject to the influence of self-gravity. These modes determine the gravitational instability in vertically stratified discs. As we have clearly seen in all the above cases, the radial scale of the instability is comparable, though a bit larger than the disc thickness, $\lambda_m \gtrsim H$, which in turn implies that a 2D analysis of the gravitational instability is at most marginally valid and the rigorous stability (linear) analysis of self-gravitating discs should be three-dimensional. However, despite the 2D treatment only being marginal, we can still find similarities between our results

and the 2D density wave theory in thin self-gravitating discs, which actually appears to do a decent qualitative job.

Consider an equivalent zero-thickness disc with the sound speed c_{sm}^1 and the surface density $\Sigma_0 = \int_{-h}^h \rho_0 dz$. Then the well-known dispersion relation of axisymmetric 2D density waves in the thin disc is (e.g., Goldreich & Tremaine 1978)

$$\omega^2 = k^2 - \frac{2}{Q_{2D}}k + 1,$$

where we have used the same normalization as before and

¹ In fact, there are other options for choosing the sound speed as a some kind of height-averaged value. We address this question in Section 6, but for the present purpose this does not make much difference.

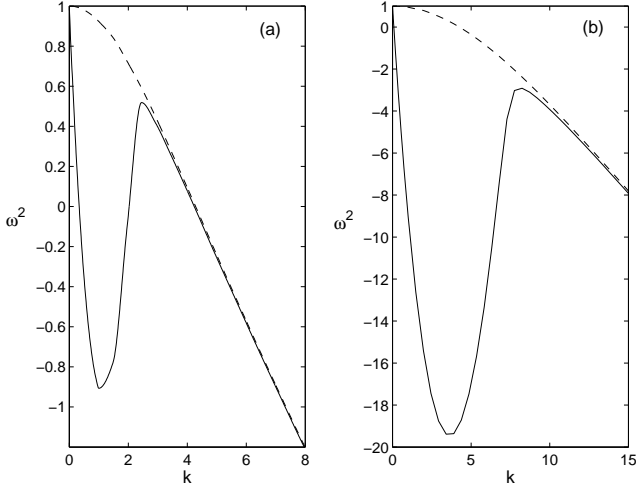


Figure 6. Dispersion curves of the basic even g-mode for a superadiabatic stratification with $s = 1.7$ for (a) $Q = 0.1$ and (b) $Q = 0.01$. Dashed lines show the same branches computed without self-gravity in the perturbations. For $Q = 0.1$, the basic even g-mode exhibits gravitational instability in the vicinity of $k_m = 1.15$ and convective instability in the range $k > 4.27$, where the influence of self-gravity is weak. For $Q = 0.01$, the effect of self-gravity is much stronger and the radial scales of gravitational and convective instabilities overlap in the range $4.25 \leq k \leq 8.5$.

because of that $Q_{2D} = c_{sm}\Omega/\pi G\Sigma_0$. This dispersion relation is a parabola with a minimum at the Jeans wavenumber $k_J = 1/Q_{2D}$. This is the wavenumber, at which the effect of self-gravity is most prominent, and if $Q_{2D} < 1$ it gives the characteristic scale of gravitational instability. At small $k \ll k_J$, 2D density waves are dominated by self-gravity and inertial forces, while at large $k \gg k_J$, pressure/compressibility dominates over self-gravity and density waves appear as an acoustic mode. At $k \sim k_J$ all three factors can be important. Let us now look at the dispersion curves of the basic branches of the even r- and convectively unstable even g-modes in Figs. 3c,5c,5g. They have similar parabolic shape in the self-gravity and compressibility dominated regime at $k \sim k_m$ with the linear phase at smaller $k \ll k_m$, where only self-gravity and inertial forces play a role. This linear phase at long wavelengths is well reproduced by the 2D dispersion relation. Therefore, we can identify the wavenumber k_m , at which the effect of self-gravity on the 3D modes is largest, with the Jeans wavenumber k_J . In some sense, in the case of instability when $Q < Q_{cr}$, k_m gives a more accurate value for the radial scale, λ_m , of the gravitationally most unstable mode than that given by the Jeans wavenumber k_J in the 2D model. For example, from Fig. 12 we find that the vertical structure (ρ_0) calculated at $s = 5$ and $Q_{cr} = 0.168$ gives the corresponding $Q_{2D} = 0.76$ and $k_J = 1.32$, which differs from $k_m = 0.8$ found above for these parameters. Moreover, we will see in Section 6 that the criterion for gravitational instability based on the 3D calculations, i.e. $Q < Q_{cr}$, is more exact than the 2D criterion $Q_{2D} < 1$.

In the 2D case, as shown above, the Jeans wavenumber $k_J = 1/Q_{2D}$, implying that it is determined solely by competition between self-gravity and compressibility/pressure. It is now interesting to see how an analogous characteristic

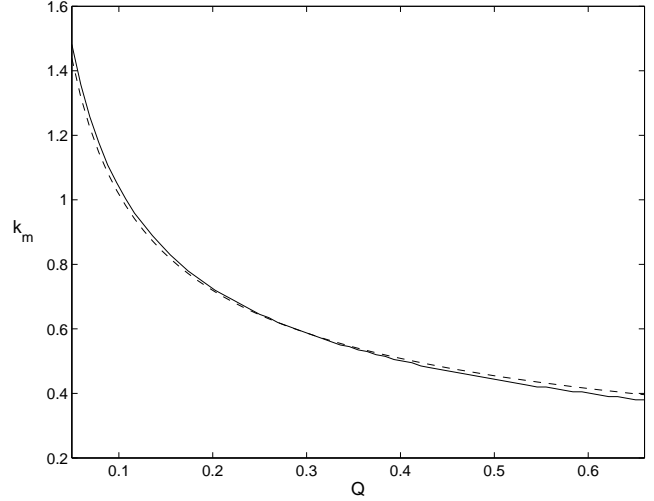


Figure 7. Dependence of k_m on Q for $s = 5$, which very closely follows the power law $Q^{-1/2}$ (shown with dashed line and scaled appropriately). The gravitational instability sets in at $Q = Q_{cr} = 0.168$ that gives $k_m = 0.8$.

wavenumber k_m depends on Q in the 3D case. From Fig. 7 we see that this dependence has a power law character $Q^{-1/2}$, which means that the value of k_m is again set by self-gravity and compressibility, as in the 2D case, so that the disc rotation plays a role only in determining ω^2 but not k_m . Indeed, the only lengthscale that can be constructed from the sound speed c_{sm} , density ρ_m and gravitational constant G without the angular velocity, Ω , of disc rotation is $c_{sm}/\sqrt{G\rho_m}$ (analogous to the Jeans length of a collapsing 3D cloud). If we normalize it by c_{sm}/Ω , we get $2\sqrt{\pi}Q^{1/2}$, giving the above power law dependence for the corresponding non-dimensional wavenumber $\sqrt{\pi}Q^{-1/2}$ to which k_m is proportional.

Thus, the basic even r-mode or, in the case of superadiabatic stratification, the basic even g-mode at $k \lesssim k_m$ exhibit many of the characteristics of 2D density waves and could be regarded as their 3D analogues at such radial wavenumbers (see also Section 5). If continued to $k \gg k_m$, the density wave mode would thus connect up to the large- k parts of these two modes dominated, respectively, by inertial forces and by negative buoyancy, instead of merging with the compressible p-mode, as might seem at first sight from the 2D dispersion relation. However, the limit $k \gg k_m$, equivalent to $\lambda \ll H$, means the breakdown of the 2D approximation and, therefore, the concept of 2D density waves at $k \gg k_m$ would not be well-defined.

5 GRAVITATIONAL INSTABILITY IN 3D: PROPERTIES OF THE BASIC BRANCH OF THE LOW-FREQUENCY EVEN R-MODE

In this section we concentrate only on the properties of the gravitationally unstable basic even r-mode. As we have seen, the behaviour of the convectively unstable basic even g-mode under self-gravity has a qualitatively similar character.

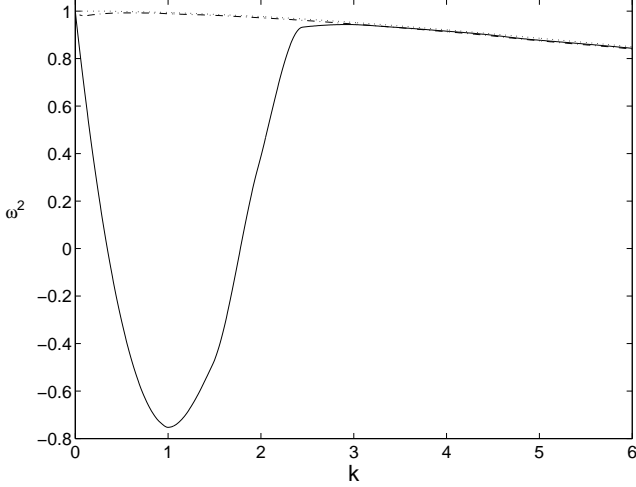


Figure 8. Dispersion curves of the basic even r-mode at $s = 5, Q = 0.1$ with corresponding $h = 1.22$. Dotted line corresponds to the non-self-gravitating case, dashed-dotted – to the incompressible case with self-gravity and solid line – to the self-gravitating case with compressibility. The influence of self-gravity on the basic even r-mode is very weak in the incompressible limit and the dashed-dotted dispersion curve almost coincides with the dotted one in the non-self-gravitating limit; a slight deviation (dip) at small k is due to the stratified background.

5.1 Effect of compressibility

As noted above, in the Poisson's equation, the density perturbations giving rise to the gravitational potential perturbations can be due to compressibility and due to the stratification of the equilibrium vertical structure. As is evident from Fig. 2c, in non-self-gravitating discs, the r-mode is nearly incompressible. So, it is interesting to see if it still remains incompressible in self-gravitating discs and which out of these two sources of density perturbations is ultimately responsible for the gravitational instability. In order to explore this, we again computed the dispersion curve of the basic even r-mode in the incompressible limit of equations (16-18), which take the form:

$$\frac{du_z}{dz} = \frac{k^2}{\omega^2 - \kappa^2}(p + \psi) \quad (23)$$

$$\frac{dp}{dz} = \frac{N_0^2}{g_0}p + (\omega^2 - N_0^2)u_z - \frac{d\psi}{dz} \quad (24)$$

$$\frac{d^2\psi}{dz^2} - k^2\psi = \frac{\rho_0}{Q} \frac{N_0^2}{g_0}u_z. \quad (25)$$

supplemented with the same boundary conditions. Notice that on the right hand side of Poisson's equation (25), only the density perturbation due to stratification remains. In Fig. 8, we compare the dispersion curves of the basic even r-mode obtained in the incompressible limit to those computed for the compressible self-gravitating and non-self-gravitating cases. It is clear that in self-gravitating discs, the basic even r-mode becomes compressible at $k \sim k_m$ thereby providing density perturbation for the gravitational potential and, therefore, accounting for the large dip on the dispersion curve. The dispersion curve in the incompressible limit deviates only very slightly from that in the non-self-gravitating case, because of the second source of density

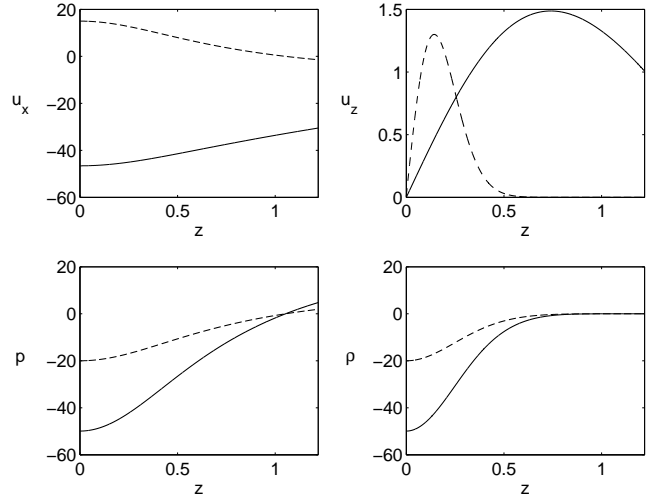


Figure 9. Vertical structures of the radial velocity u_x , the vertical velocity u_z , the pressure p and the density ρ perturbations constituting the eigenfunctions of the gravitationally unstable basic even r-mode for $s = 5, Q = 0.1, h = 1.22, k_m = 1$ with the corresponding largest growth rate $\omega_{min}^2 = -0.75$. Dashed lines show the eigenfunctions (scaled arbitrarily for plotting purposes) in the non-self-gravitating case for the same parameters except $\omega^2 = 0.99$. Notice that in the non-self-gravitating case, the eigenfunctions are more concentrated near the midplane, whereas in the self-gravitating case they vary over the whole vertical extent.

perturbation, i.e. stratification, which turns out to be much smaller than that associated with compressibility. Such a comparison also shows that the primary cause of gravitational instability in incompressible discs, as described in GLB and Lubow & Pringle (1993a), is the displacements of free-surfaces. In our case, the equilibrium density vanishes at the surface, so that the effect of surface displacements on the growth rate of instability is null (see boundary condition 22) and in the incompressible case only density perturbation due to stratification, as shown, is hardly sufficient for gravitational instability.

5.2 Eigenfunctions and spatial structure

Here we compute the vertical structure of the eigenfunctions of the gravitationally unstable basic even r-mode and also find what type of motions it induces. We take $Q = 0.1$ and $s = 5$, which gives $h = 1.22$ for the disc height. For these parameters, the dispersion curve of this mode in Fig. 8 has a minimum $\omega_{min}^2 = -0.75$, i.e. gives the largest growth rate of gravitational instability, at $k_m = 1$. In Fig. 9, we plot the corresponding eigenfunctions only in the upper half of disc's full vertical extent. Because the mode has even parity, the vertical velocity and the derivative of the gravitational potential are odd functions and, correspondingly, the pressure and potential are even functions of z . Only the pressure perturbation has one node in the interval $0 < z \leq h$, other quantities have no nodes and vary over the whole vertical extent. This demonstrates that the spatial structure of the gravitationally most unstable mode is three-dimensional with non-zero vertical velocity. To see how self-gravity changes the form of the eigenfunctions, we also show the eigenfunctions of the same branch in the non-self-gravitating limit, which

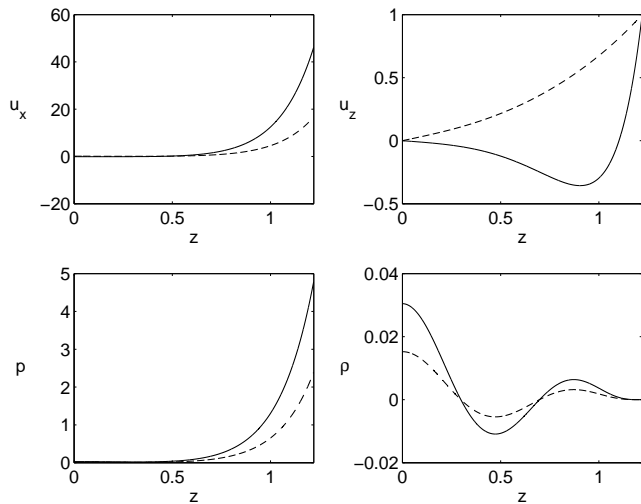


Figure 10. Eigenfunctions of the even f-mode, which unlike the basic even r-mode is gravitationally stable, with the same values of parameters as in Fig. 9. The corresponding eigenfrequencies at $k_m = 1$ are $\omega^2 = 1.1$ for the self-gravitating case (solid lines) and $\omega^2 = 1.6$ for the non-self-gravitating case (dashed lines). Again, non-self-gravitating eigenfunctions have been scaled arbitrarily for plotting purposes.

appear to be more concentrated towards the midplane than the self-gravitating ones and have no nodes in the same vertical range. Since the f-mode plays an important role in the angular momentum and energy transport in stratified discs (LO98), in Fig. 10 we also plot its eigenfunctions in the presence of self-gravity for the same parameters. Comparing Figs. 9 and 10, we clearly see that self-gravity modifies the form of the eigenfunctions of both the f- and r-modes. The perturbed quantities for both mode types vary with height somewhat similarly, especially the vertical velocities, which are, however, still at least an order of magnitude less than the horizontal ones, so that the motions can be viewed, to leading order, as 2D (see also Fig. 11). Thus, the gas motion associated with the gravitationally unstable r-mode is of similar type to that of the f-mode, which, in turn, implies that the r-mode might be as important as the f-mode, i.e., might be able to do similar ‘dynamical jobs’ as the f-mode in self-gravitating discs. As mentioned earlier, the non-linear behaviour of the 3D perturbations in self-gravitating discs has been attributed solely to the f-mode dynamics without analysing other modes (Pickett et al. 2000; Boley & Durisen 2006).

The perturbed quantities have the form $f(z)\exp(ik_mx)$, $f \equiv (u_x, u_z, p, \rho)$ and from this we can construct the spatial picture of the velocity, density and temperature perturbations for the gravitationally unstable basic even r-mode by taking the real parts. The temperature perturbation is found from the ideal gas equation of state and is equal to $T = -c_s^2 \rho / \rho_0 + \gamma p / \rho_0$ (here the pressure perturbation p is as used in the original equations 10-15, i.e., before switching to new variables). Figure 11 shows the density and temperature fields constructed in this way with velocity vectors showing the direction of gas motion superimposed on the density field, which in fact resembles the classical density profile of a 2D density wave. Near the midplane, matter flows (converges), almost parallel to the

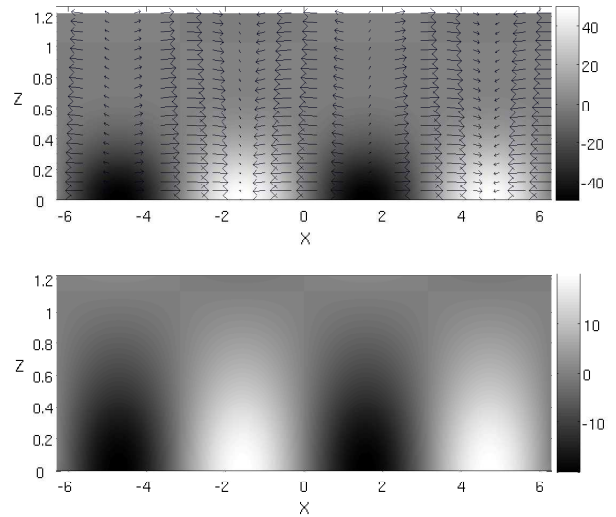


Figure 11. Distribution of the density (upper plot) and temperature (lower plot) perturbations in (x, z) plane constructed from the eigenfunctions of the gravitationally unstable basic even r-mode in Fig. 9. Superimposed on the density field are the velocity vectors of the induced gas flow.

x -axis, towards high density regions. With increasing z , the flow becomes more arc-like, because of the variation of the vertical velocity with height. An analogous velocity field in the (x, z) plane was also observed in some non-linear simulations of self-gravitating discs (Boley & Durisen 2006; Boley et al. 2006), which suggests that the latter may be a result of the non-linear development of the type of motion we see here in the linear regime. We might also speculate that in relatively high-mass discs, the non-axisymmetric gravitationally unstable basic r-mode will produce similar high-density regions, which can be precursors of spiral shock fronts (if the disc does not fragment), and arc-like motions in the upper layers that can give rise to non-linear shock bores involving large distortions of the disc surface as described by Boley & Durisen (2006). The temperature perturbations are fairly non-uniform as well, varying both vertically and radially on comparable scales. Obviously, larger temperature perturbations correspond to overdense regions that are contracting because matter flows into them, and lower – to underdense regions.

6 STABILITY CRITERIA IN 2D AND 3D

In the 3D case, the degree and effect of self-gravity is characterized by $Q_{3D} = \Omega^2 / 4\pi G \rho_m$, where ρ_m is the value of equilibrium density at the midplane (see also GLB), which plays here a role similar to that of the standard 2D Toomre’s parameter $Q_{2D} = c_s \Omega / \pi G \Sigma$ (Toomre 1964). However, in three-dimensional simulations, researchers often still tend to use the 2D Toomre’s parameter to characterize the onset of gravitational instability (Rice et al. 2003, 2005; Lodato & Rice 2004, 2005; Boley et al. 2006). In this section we investigate how a more general and exact 3D criterion of gravitational instability can be related to the 2D one. In general, these

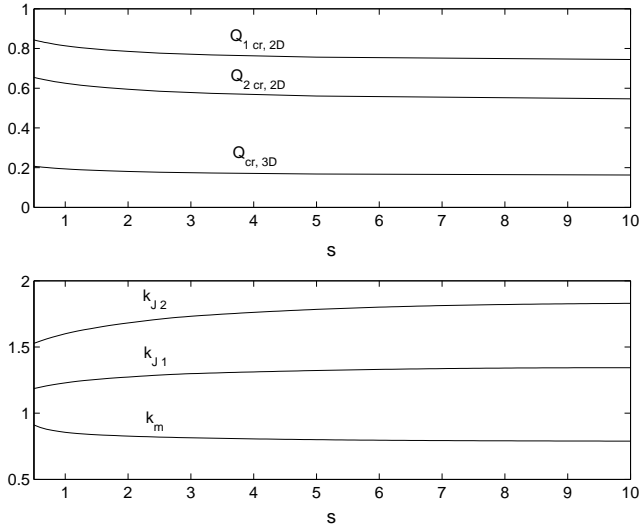


Figure 12. Dependence of the critical $Q_{cr,3D}$ and the corresponding critical $Q_{1\ cr,2D}$ and $Q_{2\ cr,2D}$ on the polytropic index s . Shown also are the k_m at $Q_{cr,3D}$ and the 2D Jeans wavenumbers $k_{J1} = 1/Q_{1\ cr,2D}$, $k_{J2} = 1/Q_{2\ cr,2D}$ as a function of s .

two parameters are different, because the 2D parameter contains the sound speed and surface density, which by definition do not vary vertically for razor-thin discs, whereas the 3D parameter does not contain the sound speed and surface density, but the midplane value of the density. So, if we still want to characterize the 3D instability in terms of the 2D Toomre's parameter, we need to use some height-averaged, or effective sound speed (surface density can be uniquely calculated from the vertical density distribution). In some simulations the midplane values (Mejía et al. 2005; Boley et al. 2006), while in others vertically averaged values (Rice et al. 2003, 2005) of the sound speed are used. Here we calculate the corresponding critical $Q_{cr,2D}$ for these cases.

As is well-known, in razor-thin 2D discs, axisymmetric perturbations (density waves) are gravitationally unstable if $Q_{2D} < 1$ (Toomre 1964). Let us now find the critical $Q_{cr,3D}$ that determines the gravitational instability in 3D, which, as found in this study, is associated with the basic branches of the even parity low-frequency modes. In Fig. 12, we show the critical $Q_{cr,3D}$ as a function of the polytropic index s . Given $Q_{cr,3D}$, we can now find $Q_{1\ cr,2D}$ defined in terms of the midplane sound speed and $Q_{2\ cr,2D}$ defined in terms of the vertically averaged sound speed:

$$Q_{1\ cr,2D} = \frac{2Q_{cr,3D}}{\int_0^h \rho_0 dz}, \quad Q_{2\ cr,2D} = \frac{2Q_{cr,3D} \int_0^h c_s dz}{h \int_0^h \rho_0 dz},$$

where ρ_0 and c_s , as before, are the normalized equilibrium density and sound speed the z -dependence of which, as well as the value of h , are determined by $Q_{cr,3D}$ and the polytropic index s . So, the critical $Q_{1\ cr,2D}$ and $Q_{2\ cr,2D}$ calculated with the two different methods are different, though not far from each other, and less than unity which is their critical value in the 2D case. This again confirms the well-known result that 3D discs are more stable and to make them unstable smaller value of Q_{2D} is necessary when compared with that required for razor-thin 2D discs (see also GLB). But in such cases, using Q_{3D} seems more appropri-

ate as it does not involve uncertainties in how to average the sound speed over height.

In Fig. 12 we also examine the dependence of the critical wavenumbers of the gravitational instability on s . We see that the 2D Jeans wavenumbers are always larger than the actual more exact wavenumber k_m at the onset of gravitational instability when $Q = Q_{cr,3D}$. Thus, in the 3D case, the critical wavenumbers depend differently on the thermodynamics than in the 2D case, where the critical $k_J = 1/Q_{2D} = 1$ at the onset of instability.

7 SUMMARY AND DISCUSSIONS

In this paper, we have analysed the axisymmetric normal modes of perturbations in stratified, compressible, self-gravitating gaseous discs with subadiabatic, adiabatic and superadiabatic vertical stratifications. First, we performed a classification of perturbation modes in stratified discs in the absence of self-gravity to compare with previous calculations. Four well-known main types of modes can be distinguished: acoustic p-modes, surface gravity f-modes, buoyancy g-modes and inertial r-modes. The restoring forces for these modes for large radial wavenumbers are mainly provided by one the following: pressure/compressibility, displacements of the disc surface, buoyancy and inertial forces due to disc rotation for the p-, f-, g- and r-modes, respectively. For smaller wavenumbers, the restoring force for each mode is a combination of these forces. In the case of adiabatic stratification, buoyancy is zero and, therefore, the g-mode disappears, while other modes remain qualitatively unchanged. For superadiabatic stratification, the g-mode becomes convectively unstable and merges with the r-mode, so that only a single convectively unstable mode appears in the dispersion diagram at $\omega^2 \leq \kappa^2$, which we still call the g-mode. Due to the reflection symmetry of the equilibrium vertical structure with respect to the midplane, each mode comes in even and odd pairs. By our terminology, for even (odd) modes, pressure and gravitational potential perturbations are even (odd), while the perturbations of vertical velocity and derivative of potential are odd (even) functions of the vertical coordinate. After classifying and characterizing modes in the absence of self-gravity, we introduced self-gravity in the perturbation equations and investigated how it modifies the properties of these modes. We found that self-gravity, to some extent, reduces the frequencies of all normal modes at radial wavelengths comparable to the disc height, but its influence on the basic even r-mode, in the case of subadiabatic and adiabatic stratifications, and on the basic even g-mode, in the case of superadiabatic stratification, appears to be strongest. With decreasing Q_{3D} , these modes become unstable due to self-gravity and thus determine the gravitational instability of a vertically stratified disc. The basic even g-mode also exhibits convective instability due to a negative entropy gradient but, unless the disc is strongly self-gravitating, these two instabilities grow concurrently in the linear regime, because their corresponding radial scales are separated. We also obtained the corresponding criterion for the onset of gravitational instability in 3D, which is more exact than the standard instability criterion in terms of the 2D Toomre's parameter, $Q_{2D} < 1$, for axisymmetric density waves in razor-thin discs. By contrast, the

p-, f- and convectively stable g-modes have their ω^2 reduced by self-gravity, but never become unstable for any value of Q_{3D} . This is a consequence of the three-dimensionality of the disc. The eigenfunctions associated with the gravitationally unstable modes are intrinsically three-dimensional, that is, have non-zero vertical velocity and all perturbed quantities vary over the whole vertical extent of the disc. In this regard, we would like to mention that resolving the gravitationally most unstable mode in numerical simulations thus reduces to properly resolving the disc height (together with resolving the corresponding radial scale, which, as shown here, appears somewhat larger than the disc height). So, the criterion of Nelson (2006) that at least ~ 4 particle smoothing lengths should fit into per scale height may apply in three-dimensional SPH simulations. This implies a substantially larger number of SPH particles per vertical column because the disc itself may extend over many scale heights. He also shows that a similar criterion applies to grid-based simulations.

Here for simplicity, and also to gain the first insight into the effects of self-gravity on the vertical modes in stratified discs, we considered only axisymmetric perturbations. Non-axisymmetric perturbations are dynamically richer, though more complicated, because the phenomena induced by Keplerian shear/differential rotation – strong transient amplification of perturbations and *linear* coupling of modes (not to be confused with non-linear mode-mode interactions) – come into play for these type of perturbations. Transient (swing) amplification of perturbations (density waves) has been studied previously in razor-thin 2D approximation (Goldreich & Lynden-Bell 1965b; Goldreich & Tremaine 1978; Toomre 1981; Mamatsashvili & Chagelishvili 2007). From the analysis presented here, we may expect that in the linear regime, the non-axisymmetric basic even r-mode can undergo larger transient amplification due to self-gravity than other modes in the disc. This transient amplification of perturbations may be important for explaining the large burst phases seen in numerical simulations at the initial stages of the development of gravitational instability in discs (Rice et al. 2003, 2005; Lodato & Rice 2004, 2005; Boley et al. 2006). So, in this respect one should analyse and quantify the transient amplification of non-axisymmetric perturbations in stratified 3D self-gravitating discs starting with linear theory. As for the linear coupling of modes, it was demonstrated that in non-self-gravitating stratified discs, Keplerian shear causes rotational (vortex) mode perturbations to couple with and generate g-mode perturbations (Tevzadze et al. 2008). In the context of 2D discs, it was shown that vortex mode perturbations can also excite density waves due to shear (Bodo et al. 2005; Mamatsashvili & Chagelishvili 2007; Mamatsashvili & Rice 2009; Heinemann & Papaloizou 2009). In the 3D case, there are a larger number of modes in a disc and it is quite possible that some of them may appear linearly coupled due to shear and, therefore, be able to generate each other during evolution, especially the f-mode and the basic branch of the r-mode (because they vary on comparable vertical scales in the presence of self-gravity, Figs. 9, 10). Another related problem also of interest is the interaction between self-gravity and the MRI in magnetized discs (see e.g., Fromang 2005). In particular, how self-gravity can modify the growth rates of magnetic normal modes responsible for the MRI. Actu-

ally, this will be the generalization of the extensive analysis of normal modes in magnetized discs by Ogilvie (1998).

Lubow & Ogilvie (1998) showed that in non-self-gravitating discs with polytropic vertical stratification, an external forcing preferentially excites the f-mode, because it has the largest responsiveness to an external driving compared to other modes. This mode, propagating through a disc, results in energy dissipation near the disc surface. Based on these results and partly on the properties of f-modes in stellar dynamics, Pickett et al. (2000) identified the behaviour of 3D perturbations in self-gravitating discs involving large surface distortions and the resulting energy dissipation in the upper layers, with f-mode dynamics. The self-stimulated potential was thought to play the role of an external/tidal force. However, it is not obvious that the effect of a self-stimulated potential is the same as that of the external potential. In fact, our analysis has revealed that in self-gravitating discs, in addition to the f-mode, the r-mode can also be dynamically important, because this mode appears to be subject to gravitational instability, while the f-mode is not. The eigenfunctions of the gravitationally unstable basic even r-mode differ from those of the r-mode in non-self-gravitating discs in that they are no longer concentrated near the midplane and behave somewhat similarly to the eigenfunctions of the f-mode: they vary over the whole vertical extent of the disc and also involve noticeable perturbations of the disc surface. Consequently, like the f-mode, the gravitationally unstable r-mode can, in principle, also induce gas motion causing large surface distortions and resultant energy dissipation in the upper layers of the disc, which is thought to play a role in enhancing disc cooling (because the energy is deposited in the upper layers with small optical depth, it can be radiated away more quickly and effectively cool the disc, but this is a subject of further study, see e.g., Johnson & Gammie 2003; Boley et al. 2006). Furthermore, in the case of non-axisymmetric perturbations, as mentioned above, because of shear, the gravitationally unstable r-mode can couple with and generate the strong f-mode. So, the surface distortions may be caused by a combination of the f- and r-modes. In order to explore where dissipation can predominantly occur in a self-gravitating disc, one needs to generalize the analysis of Lin et al. (1990), LP, LO98, Bate et al. (2002) on the propagation of waves in stratified non-self-gravitating discs and consider the propagation of non-axisymmetric modes in stratified self-gravitating discs. The dispersion properties of modes in the presence of self-gravity as found here are one of the necessary things for studying mode propagation.

Another point we want to raise concerns the spatial distribution of temperature. In order to realistically model the cooling of protoplanetary discs, Boley et al. (2007) employed the radiative transfer technique. In the vertical z -direction, the radiative transfer equation was solved exactly assuming a plane-parallel atmosphere approximation, but in the radial direction only the radiation diffusion approximation was employed. However, as our linear results (Fig. 11) and other non-linear simulations (e.g., Mejía et al. 2005; Boley et al. 2006) demonstrate, temperature and, therefore, opacity may vary on comparable scales in both the radial and vertical directions and have very complex structure in the non-linear regime. This implies that a more general radiative transfer treatment based on solving the ray equation in all directions,

rather than using the diffusion approximation in either direction, would be more appropriate for better understanding cooling processes.

ACKNOWLEDGMENTS

G.R.M. would like to acknowledge the financial support from the Scottish Universities Physics Alliance (SUPA). We thank Gordon Ogilvie for helpful discussions and for critically reading the manuscript. We also thank the referee for the constructive comments that improved the presentation of our results.

REFERENCES

- Adams F. C., Ruden S. P., Shu F. H., 1989, *ApJ*, 347, 959
 Bate M. R., Ogilvie G. I., Lubow S. H., Pringle J. E., 2002, *MNRAS*, 332, 575
 Bertin G., Lin C. C., Lowe S. A., Thurstans R. P., 1989, *ApJ*, 338, 104
 Binney J., Tremaine S., 1987, *Galactic dynamics*. Princeton University Press, Princeton, NJ
 Bodo G., Chagelishvili G., Murante G., Tevzadze A., Rossi P., Ferrari A., 2005, *A&A*, 437, 9
 Boley A. C., 2009, *ApJ*, 695, L53
 Boley A. C., Durisen R. H., 2006, *ApJ*, 641, 534
 Boley A. C., Durisen R. H., Nordlund Å., Lord J., 2007, *ApJ*, 665, 1254
 Boley A. C., Mejía A. C., Durisen R. H., Cai K., Pickett M. K., D'Alessio P., 2006, *ApJ*, 651, 517
 Boss A. P., 1998, *ApJ*, 503, 923
 Boss A. P., 2003, *ApJ*, 599, 577
 Boss A. P., 2004, *ApJ*, 610, 456
 Fromang S., 2005, *A&A*, 441, 1
 Gammie C. F., 2001, *ApJ*, 553, 174
 Goldreich P., Lynden-Bell D., 1965a, *MNRAS*, 130, 97
 Goldreich P., Lynden-Bell D., 1965b, *MNRAS*, 130, 125
 Goldreich P., Tremaine S., 1978, *ApJ*, 222, 850
 Heinemann T., Papaloizou J. C. B., 2009, *MNRAS*, 397, 52
 Johnson B. M., Gammie C. F., 2003, *ApJ*, 597, 131
 Korycansky D. G., Pringle J. E., 1995, *MNRAS*, 272, 618
 Laughlin G., Bodenheimer P., 1994, *ApJ*, 436, 335
 Laughlin G., Korchagin V., Adams F. C., 1997, *ApJ*, 477, 410
 Lin D. N. C., Papaloizou J. C. B., Savonije G. J., 1990, *ApJ*, 364, 326
 Lodato G., Rice W. K. M., 2004, *MNRAS*, 351, 630
 Lodato G., Rice W. K. M., 2005, *MNRAS*, 358, 1489
 Lubow S. H., Ogilvie G. I., 1998, *ApJ*, 504, 983
 Lubow S. H., Pringle J. E., 1993a, *MNRAS*, 263, 701
 Lubow S. H., Pringle J. E., 1993b, *ApJ*, 409, 360
 Mamatsashvili G. R., Chagelishvili G. D., 2007, *MNRAS*, 381, 809
 Mamatsashvili G. R., Rice W. K. M., 2009, *MNRAS*, 394, 2153
 Mayer L., Lufkin G., Quinn T., Wadsley J., 2007, *ApJ*, 661, L77
 Mejía A. C., Durisen R. H., Pickett M. K., Cai K., 2005, *ApJ*, 619, 1098
 Nelson A. F., 2006, *MNRAS*, 373, 1039
 Ogilvie G. I., 1998, *MNRAS*, 297, 291
 Papaloizou J. C., Savonije G. J., 1991, *MNRAS*, 248, 353
 Papaloizou J. C. B., Lin D. N. C., 1989, *ApJ*, 344, 645
 Pickett B. K., Cassen P., Durisen R. H., Link R., 2000, *ApJ*, 529, 1034
 Pickett B. K., Mejía A. C., Durisen R. H., Cassen P. M., Berry D. K., Link R. P., 2003, *ApJ*, 590, 1060
 Rafikov R. R., 2007, *ApJ*, 662, 642
 Rice W. K. M., Armitage P. J., Bate M. R., Bonnell I. A., 2003, *MNRAS*, 339, 1025
 Rice W. K. M., Lodato G., Armitage P. J., 2005, *MNRAS*, 364, L56
 Romeo A. B., 1992, *MNRAS*, 256, 307
 Romeo A. B., 1994, *A&A*, 286, 799
 Ruden S. P., Papaloizou J. C. B., Lin D. N. C., 1988, *ApJ*, 329, 739
 Shu F., 1968, PhD thesis, Harvard University, Cambridge, Massachusetts, USA
 Stamatellos D., Whitworth A. P., 2009, *MNRAS*, 400, 1563
 Tevzadze A. G., Chagelishvili G. D., Zahn J., 2008, *A&A*, 478, 9
 Toomre A., 1964, *ApJ*, 139, 1217
 Toomre A., 1981, in S. M. Fall & D. Lynden-Bell ed., *Structure and Evolution of Normal Galaxies*. Cambridge University Press, Cambridge